Modeling of stator versus magnet width effects in high-T_c superconducting dynamos

Ratu Mataira, Mark D. Ainslie, *Senior Member, IEEE*, Rod Badcock, *Senior Member, IEEE*, and Chris W. Bumby

***Abstract*—High-T_c superconducting (HTS) dynamos are simple devices for injecting and sustaining dc currents in superconducting coils/magnets. The simple geometry of these devices consists of a superconducting stator(s) and one or more rotor magnets arranged in identical fashion to a classical alternator. However, unlike the classical alternator, the HTS dynamo gives a self-rectified dc output. This somewhat anomalous result is caused by the non-linear resistivity of HTS materials and the large over-critical eddy currents that flow in the stator. As these over-critical currents must recirculate in the HTS stator, the stator's width becomes a key parameter in the physics of the device. In this work we explore the effect of increasing the stator width through using recent advances in modeling these systems. We find that given enough space in the stator, the total sum of circulating and transport currents do not drive the full width of the stator into the flux-flow regime. Operation of the device in this regime results in a non-linear I-V curve, a marked decrease in the internal resistance at open circuit R_{oc}, a saturation of the open circuit voltage V_{oc}, and a short-circuit current I_{sc} that approaches the in-field critical current of the stator itself $I_{c,min}$. These behaviors lead to the conclusion that optimal HTS dynamo design should ensure that the stator width be sufficient to avoid current saturation of the superconductor at the target operating current .**

***Index Terms*—Flux pump, HTS dynamo, coated conductor, current leads, YBCO, superconducting generator.**

I. Introduction

HIGH-T_c superconducting (HTS) dynamos [1]–[11], are a subclass of HTS flux pump [12]–[19], which have attracted significant recent interest [20]–[25]. The HTS dynamo is topologically identical to a standard ac alternator, but the use of an HTS coated conductor (CC) for the stator wire has the dramatic effect of making these devices partially self rectifying; that is, they generate a net dc output V_{dc}. Using this dc voltage, this inherently superconducting device can inject dc current into a superconducting coil, without the use of copper current leads and their associated losses [26]. The origin of the rectification effect in the HTS dynamo is not trivial to explain, as unlike a bridge rectifier device [4], [13], [17], [18], HTS dynamos do not include a separate switching element. Instead, a simple dynamo only has a single circuit element, namely the stator wire itself. However, the 2D planar geometry of an HTS Coated conductor stator allows for non-trivial internal currents to flow within the stator. Depending on their absolute magnitude, these currents experience a varying local resistivity due to the highly nonlinear behavior of the HTS film. It is this effect which gives rise to an auto-rectified output [5], [27], [28].

This work was supported by New Zealand MBIE Endeavour contract no. RTVU1707), and NZ Royal Society Marsden Award no. MFP-VUW1806. The work of M. D. Ainslie was supported by the Engineering and Physical Sciences Research Council (EPSRC) Early Career Fellowship EP/P020313/1.

R. Mataira, R. A. Badcock and C. Bumby are with the Robinson Research Institute, Victoria University of Wellington, PO Box 33436, Lower Hutt 5046, New Zealand. (e-mail: Chris.Bumby@vuw.ac.nz

M. Ainslie is with the Bulk Superconductivity Group, Department of Engineering, University of Cambridge, Trumpington Street, Cambridge CB2 1PZ, United Kingdom.

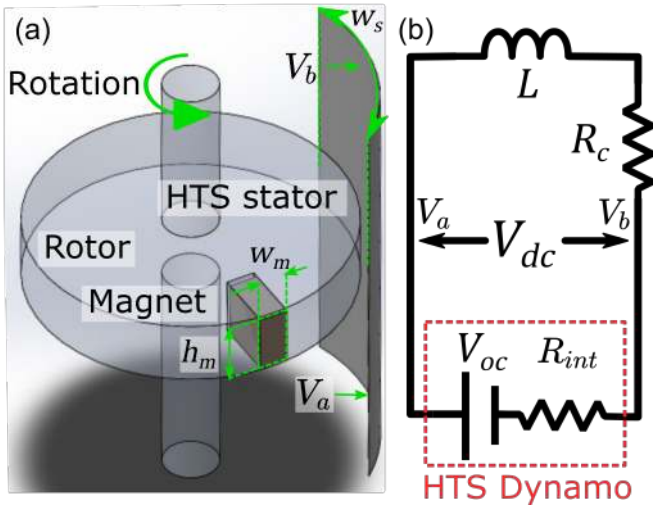

Fig. 1. (a) Schematic of the HTS dynamo modeled in this work, with a stator width of 46 mm. (b) Equivalent circuit defining the dc characterization of the device in (a), where R_c is the joint resistance to the HTS coil L.

Fig. 1 (a) shows a schematic of an HTS dynamo device similar to that modeled in [27]. Here, the model has been modified to accommodate a larger stator width, w. It has been experimentally shown that the dc characteristics of this HTS dynamo can be described by the simple circuit model [3], [7], [29] shown in Fig. 1 (b). This model describes the dynamo as a simple voltage source with an internal resistance R_{int}, and open-circuit voltage V_{oc}. In experiments, the magnetic field of the load coil can be measured to discern the net current, I flowing through the device [6]. Alternatively, an electronic power supply can be used as an artificial load to set the current [7], [30]. This along with measurements of the voltage, can be presented as the output I-V characteristic of the device, which allows V_{oc}, R_{int}= V_{dc}/I, and the short-circuit current I_{sc}= $I(V_{dc} = 0)$ to each be defined.

To understand the dc characteristics of the HTS dynamo, it is important to revisit the classical ac alternator where V_{ab} (the *emf* induced along the stator wire between points *a* and *b*) can be expressed as:

$$V_{ab} = \int_a^b -\partial_t \vec{A} \cdot d\vec{l}, \tag{1}$$

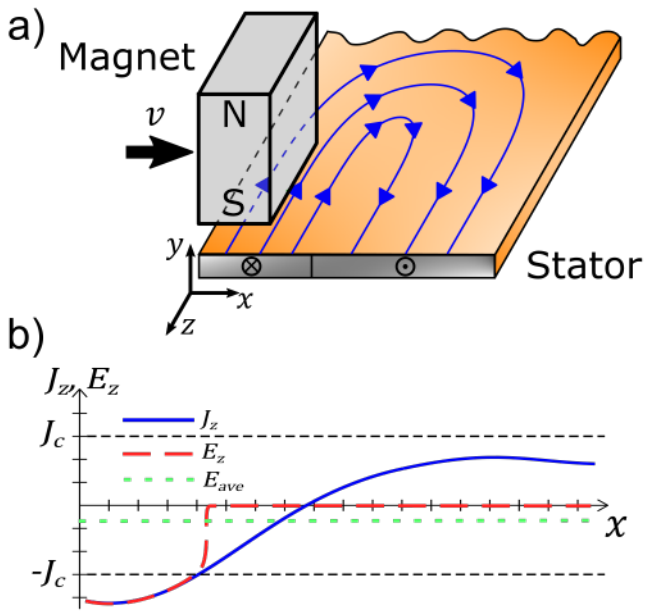

Fig. 2. (a) Illustration of the eddy currents driven by a magnet moving with velocity, v, across a conductive stator, current flow is shown in blue in the $x-z$ plane. (b) Illustration of the eddy current flows in open circuit through the cross section of the conductor. Only over-currents, $J_z > J_c$, experience a resistivity, leading to a bias in the electric field.

where $\vec{A}$ is the vector potential along the component. Taking the time average of this emf over one period, *P*, of the rotor cycle leads to the natural result that a classical ac alternator does not deliver a dc component:

$$V_{dc} = \frac{1}{P}\int_t^{t+P} V_{ab}dt = -\frac{1}{P}\int_a^b (\vec{A}(t+P) - \vec{A}(t)).d\vec{l} = 0, \quad (2)$$

as $\vec{A}$ imposed by the rotor magnet is periodic.

In order to understand why this result does not hold for the HTS dynamo, it is necessary to also consider the eddy currents which flow in the plane of the stator wire as the magnet moves across it. This is depicted in Fig. 2 (a) for a rotor magnet moving across the wide face of a coated conductor wire. Wherever the applied magnetic field penetrates the conductor, emf-driven eddy currents are induced. The magnitude of the induced eddy currents is determined by the local magnitude of the applied field, such that the largest eddy currents flow directly beneath the magnet [31].

To account for the eddy current effect we must rewrite (1) to include the internal electric field which arises from the resistivity of the stator, as $\vec{E} = \rho\vec{J}$). Integrating over the full volume of the stator wire then yields:

$$V_{ab} = \frac{1}{wd}\int_{-w/2}^{w/2} dx \int_{-d/2}^{d/2} dy \int_a^b \left(-\partial_t \vec{A} - \vec{E}\right) \cdot d\vec{z}. \quad (3)$$

where w and d denote the spatial extent of the stator wire in the x- and y-directions respectively.

For the HTS dynamo, this has an important consequence as the time-averaged net dc value now includes a contribution from the average electric field across the cross section of the stator wire, E_{ave}. If the stator wire exhibits ohmic resistivity (e.g. a classical metal) then this contribution is zero in the open-circuit case [27]. However for a stator material exhibiting non-zero resistivity (such as an HTS ReBCO film) the contribution from E_{ave} will not be zero and hence cannot be neglected (see Fig. 2 (b)). Therefore, we obtain the dc voltage across the stator wire as :

$$V_{dc} = \frac{1}{P}\int_t^{t+P}\int_a^b E_{ave}dzdt, \quad (4)$$

where

$$E_{ave} = \frac{1}{wd}\int_{-w/2}^{w/2} dx \int_{-d/2}^{d/2} E_z dy. \quad (5)$$

A more detailed discussion of this effect is provided in [27]. This also provides a detailed discussion of the finite element model also used in this work to simulate the 2D currents flowing in the coated conductor stator of an HTS dynamo, and hence calculate E_{ave} and V_{dc}.

It has been shown that this FE model can reproduce experimentally observed dc output from the HTS dynamo using only the geometry of the dynamo and the non-linear resitivity of the HTS stator [27]. The model shows that large over-critical currents, $J >> J_c$ are present during the transit of the magnet across the stator wire, which are associated with the large locally-induced electric fields. However, previous work has only considered stator wires of a similar width to the rotor magnet. In this case the stator is saturated with over-critical currents (in both the forward and backward directions) for most of the magnets transit time over the stator tape. This leads to the natural question: *'Can the HTS stator be made large enough to support both the induced current from the magnet's transit, and the transport currents previously accumulated?'*. There is clear experimental evidence that increasing the stator width has a marked effect on dynamo output [6]. In this work we have applied an FE model of a simple HTS dynamo to explore the effect of this parameter on the dc output of the device, and on the internal eddy current distributions flowing within the wire.

II. Methods

The model used here is adapted from the model presented in [27] where a detailed description can be found. In brief, the numerical model employs the H-formulation [32]–[37] finite element method (FEM) for solving Maxwell's equations. The H-formulation approach has been shown to be successful in handling the highly non-linear behavior of HTS materials. H-formulation assigns edge element degrees of freedom to the auxiliary field $\vec{H}$ [34, Sec. 3], and associates the current density $\vec{J}$ to the sum of $\vec{H}$ around a given finite element, thus satisfying Ampere's law explicitly:

$$\nabla \times \vec{H} = \vec{J}. \quad (6)$$

The model then solves for $\vec{H}$ that satisfies Faraday's law:

$$\nabla \times \vec{E} = \partial_t \vec{B}, \quad (7)$$

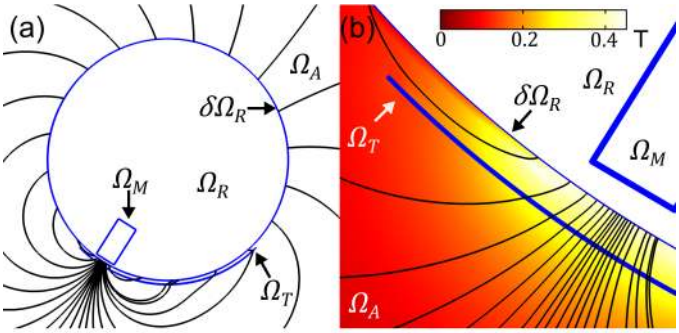

Fig. 3. Schematic illustration of the basic geometry of the 2D H-formulation model used in this work, showing the modeled cross-section of the device with a 60 mm wide stator tape. The field in the rotor domain Ω_R is not shown as it lies outside the boundary conditions of the model. (a) View of the model domains, showing magnet, rotor and tape domains (Ω_M,Ω_R, Ω_A and Ω_T respectively). (b) Magnified view of the cross section of part of the HTS stator tape Ω_T as the rotor magnet traverses the stator. Brightness corresponds with field intensity.

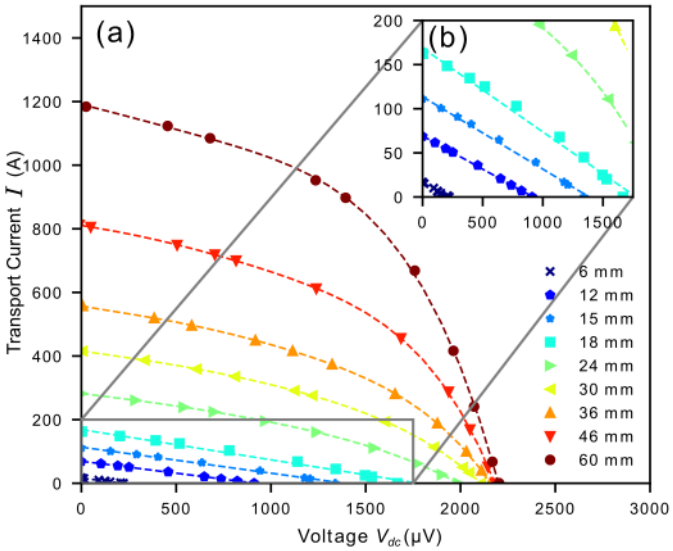

Fig. 4. I-V curves for varying widths at 38.25 Hz. (a) full I-V curves. (b) zoomed inset for 6 to 18 mm curves.

subject to the constitutive relationships $\vec{E} = \rho\vec{J}$ and $\mu\vec{H} = \vec{B}$, where $\vec{B}$ is the magnetic field; we take $\mu = \mu_0$.

The FE model is magnetically isolated at its outer boundary (the outer boundary of the air domain $\partial\Omega_A$). The geometry is simplified to 2D and captures the cross-section of the HTS tape and rotating magnet, see Fig. 3. This 2D approximation reduces the model to consider only the in-plane components of $\vec{H}$, namely H_x and H_y. Likewise it restricts analysis of $\vec{E}$ and $\vec{J}$ to their out of plane components E_z and J_z, respectively.

To solve the issue of a moving magnetic field in the H-formulation, we use a current shell method that represents the magnet Ω_M as a current density on the boundary of the rotor domain $\partial\Omega_R$. This is done by calculating the shielding currents J_s on $\partial\Omega_R$ that would completely contain the field from the magnet. The opposite shielding currents are then applied using a weak condition to the boundary $\partial\Omega_R$ in the full problem:

$$\nabla \times \vec{H} = -J_s \text{ on } \partial\Omega_R \tag{8}$$

where they reproduce the magnetic field in the domains outside of the rotor domain Ω_R. Critically this reproduces the field of the magnet in the air and stator domains, while also allowing the induced fields to pass into the rotor domain unimpeded by a Dirichlet boundary. Consequently the field in Ω_R is not physical, and is omitted from Fig. 3.

The behavior of the superconductor is captured in the E-J power law, which can be expressed as a non-linear resistivity [38], [39]:

$$\rho = \frac{E_0}{J_c}\left(\frac{J_z}{J_c}\right)^{n-1}, \tag{9}$$

where E_0 is the characteristic electric field, typically 1 μV/cm, J_c is the critical current density, and n is the flux creep exponent. J_c in HTS materials is typically a highly anisotropic function of magnetic field intensity B and direction θ_B. The index n captures the non-linear onset of dissipation in HTS materials due to flux motion and typically takes on values of 15-40 for commercially available conductor; here we take $n = 20$.

The model in this paper differs in four key respects from that reported previously. Firstly, we use a measured in-field critical current $I_c(B, \theta_B)$ function acquired from AMSC 46 mm superconducting wire, to match the wire used in Pantoja [6]. $I_c(B, \theta_B)$ data was collected from a small sample of material using the Super-Current facility at Robinson Research Institute [40], [41]. The $J_c(B, \theta_B)$ is then taken by normalizing I_c by the cross section of the modeled tape. Secondly, we sweep several values of the width w, 6, 12, 15, 18, 24, 30, 36, 46, and 60 mm. Third, for all the tape widths studied, we take a smaller flux gap $g = 2$ mm, which is selected to match B_{peak} in the model here to the device in [6] with the same width magnet, $w_m = 6$ mm, but without a magnetic yoke. And fourth, we conform the tape cross section to be concentric with the rotor, with a radius of curvature $\tau = g + r_{rotor} = 38$ mm, which keeps the flux gap constant across the full width of the stator tape. As a result, we define θ_B as the direction of the magnetic field with respect to the normal $\hat{n}$ of the curved conductor. The models are run at a relatively low rotational frequency $f = 38.25$ Hz, to enable comparison with the experimentally analogous device [6].

III. Results

Fig. 4 shows the modeled dc output from the dynamo in the form of output I-V curves for dynamos utilizing a range of different stator widths. This data was obtained by calculating the dc output obtained for each net transport current through the stator wire. In this way, the simulations produce the full I-V curve, from V_{oc} to I_{sc}. This differs from the experimental data presented in Pantoja [6], where the maximum measured current was constrained by the I_c of a series-connected load coil. The second observation in Fig. 4 is that at higher current levels, the I-V curves of the wider tapes become highly non-linear. This non-linearity has not previously been experimentally observed as it only becomes noticeable at currents above 200A - which is well above the

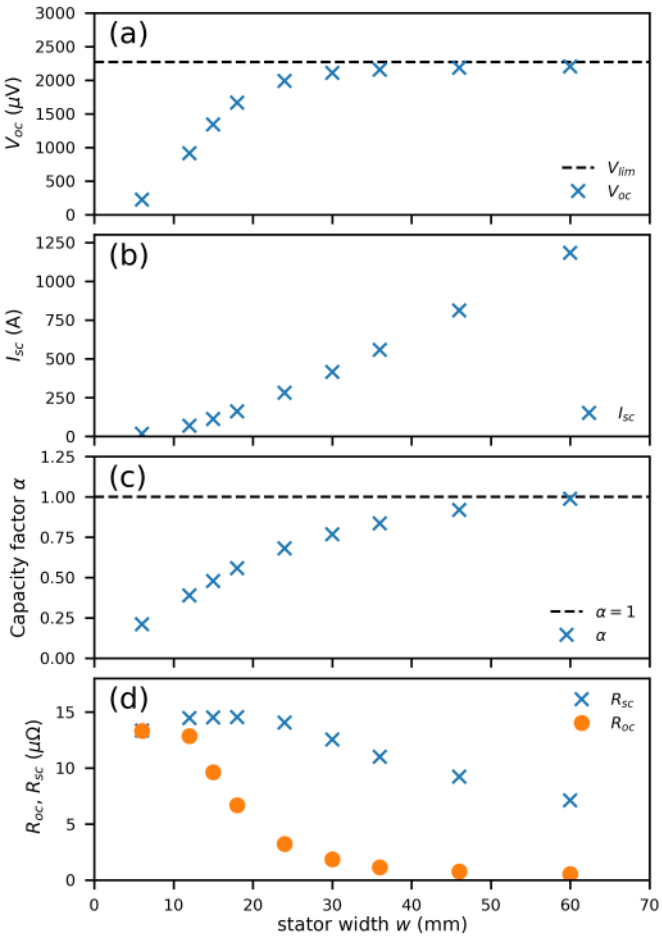

Fig. 5. Circuit parameters for varying stator width. (a) V_{oc}. (b) I_{sc}. (c) Capacity factor $\alpha = I_{sc}/I_{c,min}$.(d) differential resistance at open, R_{oc}, and short R_{sc} circuit.

limiting current of the coil used by [6], $I_{c,coil}$. It is perhaps not surprising that as the total transport current approaches the critical current of the stator wire, the intrinsically non-linear conductivity of the HTS stator causes an internal resistance within the stator wire which is no longer constant across its full operating range. Notwithstanding the above, it should also be noted (Figure 4(b)) that for narrower stator widths $\leq$18mm the $I-V$ curves remain approximately linear, which is consistent with experimental on devices using 12 mm wide coated conductor wire [3], [24], [29].

Further insight into the evolution of these I-V curves with stator width can be obtained by considering the circuit parameters defined in Fig. 1 (b), namely, V_{oc}, I_{sc} and the internal resistance of the dynamo stator, R_{int}. Fig. 5 (a) shows the evolution of the open circuit voltage V_{oc} with increasing width, which clearly approaches a limiting value V_{lim}. This mirrors the behavior in [6] for stator widths up to 46 mm; whilst the addition of modeled data at 60 mm makes the limiting behavior more apparent. One way to interpret this observation is to consider that dynamos employing narrower stators have a restricted ability to efficiently rectify the available *emf*. This is an important finding and implies that an important design rule for dynamo devices is that the width of a stator wire [6], or stator network [11], [42], [43], should be sufficiently wide to achieve the maximal *emf*, V_{lim} (in this case $w > 4w_m$). The definition of *sufficiently wide* will depend on — and influence — magnet yoke and flux gap design, which must be considered together, an investigation we leave to future work.

Fig. 5 (b) shows how the short-circuit current I_{sc} of the device increases approximately linearly with stator width. As the stator width increases, the increase in I_{sc} begins to correlate with the increase in stator I_c. To further explore this we can consider the capacity factor of the tape, α, which we define as:

$$\alpha = \frac{I_{sc}}{I_{c,min}}, \tag{10}$$

where $I_{c,min}$ is the minimum critical current of the tape during the operation of the device. Ultimately, if the device is able to drive short-circuit currents equal to the stator's own critical current, then this implies that all other resistive mechanisms in the stator must have become negligible compared to the unavoidable flux flow resistivity at I_c. Fig. 5 (c) shows that α approaches 1 for the widest tape simulated. This suggest that further increases in stator width should be expected to increase I_{sc} by an amount equal to the additional I_c of the wider stator. (Although, because I_c is a somewhat arbitrary criteria, it is possible that α could slightly exceed 1 for very wide stators in which $E_0 > 1\mu$V/cm .

As the curves in Fig. 4 are non-linear, we must consider the differential internal resistance:

$$R'(I) = -\frac{\partial V(I)}{\partial I}, \tag{11}$$

where the minus sign ensures that the resistance is positive under the polarity convention used here. Different values of the differential resistance are obtained at open circuit, $R'(0A) = R_{oc}$, and short-circuit, $R'(I_{sc}) = R_{sc}$, and these are shown in Fig 5 (d). The behavior of R_{oc} shows the most dramatic effect with stator width, where it drops from 13.3 $\mu\Omega$ for a 6 mm wide stator, to 0.53 $\mu\Omega$ at 60 mm width. This transition occurs sharply between $w = 12$ mm and $w = 24$ mm such that the majority of the resistance has vanished for greater values of w. This massive reduction in R_{oc}, coupled with the relative stability of R_{sc}, suggests that some resistive mechanism in the HTS stator can be eliminated for low currents, but reemerges for high currents.

The internal resistance of the stator wire is due to the spatial restriction of the transport current, by the eddy currents which flow around the magnet region [44]. When this transport current does not have enough space to flow, it is forced above the critical current $J_z > J_c$, generating a local resistive electric field in the stator. Furthermore, the backward eddy current (in the direction of the transport current) competes for available conductor width with the forward eddy current induced under the magnet. The resistance experienced in the forward eddy current region is responsible for generating the dc voltage, so a reduction in the size of this region also reduces the dc *emf* generation.

Fig. 6 (a) shows a snapshot of the modeled currents flowing in the 12 mm wide stator tape at open-circuit when $\theta_R = 187^o$; when the rotor magnet is positioned at the right hand edge of

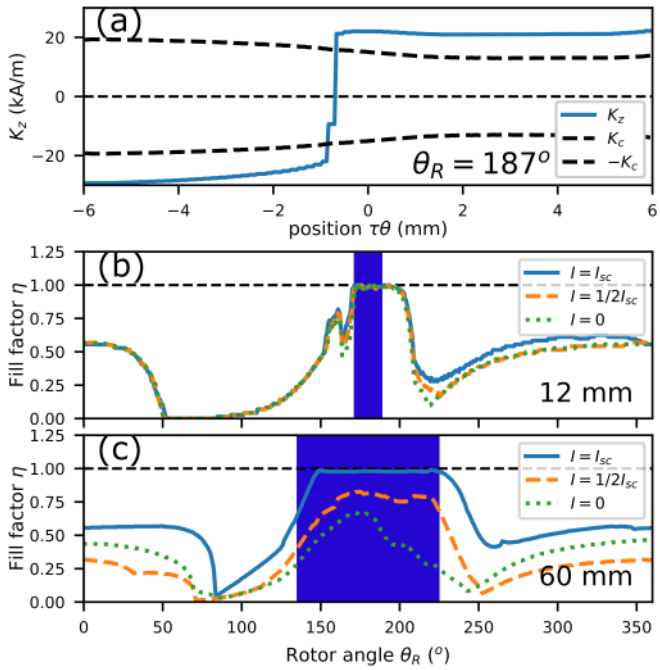

Fig. 6. (a) The sheet current density K_z and sheet critical current $\pm K_c$ for $\omega_R = 187^o$. (b) Fill factor η for the 12 mm stator across the I-V curve. (c) Fill factor η for the 60 mm stator across the I-V curve. Dark blue region denotes the location of the stator tape in (b) and (c)

the stator tape. The plot displays the sheet currents K_z and critical sheet current $\pm K_c$, at each position across the tape. These sheet currents are defined according to

$$K_z(\theta) = \int_{\tau-b}^{\tau+b} J_z(r,\theta)dr, \tag{12}$$

and

$$K_c(\theta) = \int_{\tau-b}^{\tau+b} J_c(B,\theta_B,r,\theta)dr, \tag{13}$$

where b is the half thickness of the modeled tape.

We can define a function u to express whether overcritical current is flowing at a given position across the stator tape:

$$u(K_z,K_c) = \begin{cases} 1 & \text{if } |K_z| \geq K_c \\ 0 & \text{otherwise.} \end{cases} \tag{14}$$

From this, we can then define a fill factor, η, to denote the fraction of the conductor width that contains a sheet current K_z greater than the sheet critical current K_c,:

$$\eta = \frac{1}{w_s}\int_{-w_s/2\tau}^{w_s/2\tau} u(\theta)d\theta. \tag{15}$$

Fig. 6(b) shows the fill factor η of the stator wire as a function of rotor angle θ_R for the 12 mm stator. Modeled data is shown for a full rotation of the magnet for three different transport currents which span the full I-V curve, namely I =0 (open-circuit), $I = I_{sc}$ (short-circuit) and $I = I_{sc}/2$. We see that every transport current, the fill factor of the 12 mm tape is essentially $\eta = 1$ (neglecting the small current reversal zone) during the transit of the magnet across the stator wire (blue shaded region). Fig. 6(c) shows a similar situation pertains for the 60 mm stator at I_{sc}. However, the same is not true for the 60mm stator at $I = 0A$ and $I = 1/2I_{sc}$. In both these cases η never rises above 75%, indicating that there is still ample room in the conductor width for additional transport current to flow around the eddy current region.

IV. Conclusions

The optimized design of HTS dynamo devices requires a deeper understating of their operating mechanism. In this work, we have explored the effect of increasing stator width on the key dc output parameters of the HTS dynamo. The first and most striking observation is the appearance of a non-linear I-V characteristic with increasing stator width, with the non-linear aspect most apparent at high output currents. We also observe that both V_{oc} and I_{sc} increase significantly with increasing stator width. This is attributed to a very significant (order of magnitude) reduction in the open-circuit internal resistance of the device, R_{oc}, which occurs between w =12mm and w =24mm. Once the stator width exceeds approximately four times the magnet width, we observe that V_{oc} of the device approaches a limiting maximum value V_{lim} whilst the short-circuit current I_{sc} of the dynamo starts to approach the critical current of the stator $I_{c,min}$.

The sharp reduction in R_{oc} above w =24mm, marks a distinct change in the operating mechanism of the device. Previous studies of narrow stator dynamos [27], have described the HTS dynamo in the context of large over-currents, $J >> J_c$, fully occupying the superconducting stator at all times during the magnet transit. However, the FE models used here show that, given enough space, the induced eddy currents around the moving rotor magnet can co-exist with the transport current without driving the entire stator into the flux flow regime. However, at large transport currents approaching I_{sc}, the transport and eddy currents do still compete for available space within the conductor during at least some parts of of the cycle (Fig. 6). As a result the differential resistance increases rapidly as $I \rightarrow I_{sc}$.

These findings suggest that high current HTS dynamos are quite possible, and could in fact produce larger voltages at their operating current than implied from previous linear I-V models. Furthermore it suggests that optimal dynamo designs will involve stators, or stator networks, of sufficient width to efficiently rectify the *emf* of the applied field $V_{oc} \rightarrow V_{lim}$.

Acknowledgment

The authors would like to thank Dr. Stuart Wimbush and Dr. Andres Pantoja for collecting J_c data for the AMSC wire. The Authors would like to acknowledge financial support from New Zealand MBIE Endeavour grant no. RTVU1707, and NZ Royal Society Marsden Grant no. MFP-VUW1806. Additional data related to this publication are available at the University of Cambridge data repository (https://doi.org/10.17863/CAM.48317).

References

[1] C. Hoffmann, D. Pooke, and A. D. Caplin, "Flux pump for HTS magnets," *IEEE Trans. Appl. Supercond.*, vol. 21, no. 3, pp. 1628–1631, June 2011.

[2] T. A. Coombs, J. F. Fagnard, and K. Matsuda, "Magnetization of 2-G coils and artificial bulks," *IEEE Trans. Appl. Supercond.*, vol. 24, no. 5, p. 8201005, Oct 2014.

[3] Z. Jiang, K. Hamilton, N. Amemiya, R. A. Badcock, and C. W. Bumby, "Dynamic resistance of a high-T_c superconducting flux pump," *Appl. Phys. Lett.*, vol. 105, no. 11, p. 112601, 2014.

[4] J. Geng and T. A. Coombs, "Mechanism of a high-tc superconducting flux pump: Using alternating magnetic field to trigger flux flow," *Appl. Phys. Lett.*, vol. 107, no. 14, p. 142601, 2015.

[5] C. W. Bumby, Z. Jiang, J. G. Storey, A. E. Pantoja, and R. A. Badcock, "Anomalous open-circuit voltage from a high-T_c superconducting dynamo," *Appl. Phys. Lett.*, vol. 108, no. 12, p. 122601, 2016.

[6] A. E. Pantoja, Z. Jiang, R. A. Badcock, and C. W. Bumby, "Impact of stator wire width on output of a dynamo-type HTS flux pump," *IEEE Transactions on Applied Superconductivity*, vol. 26, no. 8, pp. 1–8, Dec 2016.

[7] C. W. Bumby, R. A. Badcock, H.-J. Sung, K.-M. Kim, Z. Jiang, A. E. Pantoja, P. Bernardo, M. Park, and R. G. Buckley, "Development of a brushless HTS exciter for a 10 kW HTS synchronous generator," *Supercond. Sci. Technol.*, vol. 29, no. 2, p. 024008, 2016.

[8] S. Lee, W. Kim, Y. Kim, J. Lee, S. Park, J. Lee, G. Hong, S. Kim, J. Han, Y. J. Hwang, and K. Choi, "Persistent current mode operation of a 2g HTS coil with a flux pump," *IEEE Trans. Appl. Supercond.*, vol. 26, no. 4, p. 0606104, June 2016.

[9] R. A. Badcock, S. Phang, A. E. Pantoja, Z. Jiang, J. G. Storey, H. Sung, M. Park, and C. W. Bumby, "Impact of magnet geometry on output of a dynamo-type HTS flux pump," *IEEE Trans. Appl. Supercond.*, vol. 27, no. 4, p. 5200905, June 2017.

[10] A. M. Campbell, "A finite element calculation of flux pumping," *Supercond. Sci. Technol.*, vol. 30, no. 12, p. 125015, 2017.

[11] K. Hamilton, A. E. Pantoja, J. G. Storey, Z. Jiang, R. A. Badcock, and C. W. Bumby, "Design and performance of a "squirrel-cage" dynamo-type HTS flux pump," *IEEE Trans. Appl. Supercond.*, vol. 28, no. 4, p. 5205705, June 2018.

[12] C.-S. Lee, B. Jankó, I. Derényi, and A.-L. Barabási, "Reducing vortex density in superconductors using the 'ratchet effect'," *Nature*, vol. 400, no. 6742, pp. 337–340, 1999.

[13] M. P. Oomen, M. Leghissa, G. Ries, N. Proelss, H. . Neumueller, F. Steinmeyer, M. Vester, and F. Davies, "HTS flux pump for cryogen-free HTS magnets," *IEEE Trans. Appl. Supercond.*, vol. 15, no. 2, pp. 1465–1468, June 2005.

[14] T. Nakamura, M. Sugano, T. Doi, and N. Amemiya, "Flux pumping effect of HTS films in a traveling magnetic field," *IEEE Trans. Appl. Supercond.*, vol. 20, no. 3, pp. 1033–1036, June 2010.

[15] Z. Bai, C. Chen, Y. Wu, and Z. Zhen, "Effect of various pulse wave forms for pulse-type magnetic flux pump," *Cryogenics*, vol. 51, no. 9, pp. 530 – 533, 2011.

[16] W. Wang, F. Spaven, M. Zhang, M. Baghdadi, and T. Coombs, "Direct measurement of the vortex migration caused by traveling magnetic wave," *Appl. Phys. Lett.*, vol. 104, no. 3, p. 032602, 2014.

[17] J. Geng and T. A. Coombs, "Modeling methodology for a HTS flux pump using a 2D h -formulation," *Supercond. Sci. Technol.*, vol. 31, no. 12, p. 125015, 2018.

[18] J. D. D. Gawith, J. Ma, B. Shen, C. Li, J. Yang, Y. Öztürk, and T. A. Coombs, "An HTS power switch using YBCO thin film controlled by ac magnetic field," *Superconductor Science and Technology*, vol. 32, no. 9, p. 095007, jul 2019.

[19] A. He, C. Xue, and Y.-H. Zhou, "Switchable reversal of vortex ratchet with dynamic pinning landscape," *Applied Physics Letters*, vol. 115, no. 3, p. 032602, 2019.

[20] X. Li, C. Li, X. Zhao, X. Du, X. Nie, Y. Xiong, J. Zhao, J. Sheng, Y. Wang, M. Zhang, and W. Yuan, "Study on two different charging methods for superconducting coils in persistent current mode," *Physica C: Superconductivity and its Applications*, vol. 554, pp. 44 – 50, 2018.

[21] J. H. Kim, H. L. Quach, C. Boo, Y. S. Yoon, H. Jeon, S. Han, T. K. Ko, H. Kim, Y. Jo, H. J. Park, J. Lee, H. Lee, and H. M. Kim, "Fabrication and charging test of HTS field windings using HTS contactless rotary excitation device," *IEEE Transactions on Applied Superconductivity*, vol. 29, no. 5, p. 5203207, Aug 2019.

[22] C. Wang, P. Zhou, H. Qian, X. Nie, J. Li, T. Gong, and G. Ma, "Experimental studies of current decay in a flux pumped HTS magnet subject to travelling magnetic fields," *IEEE Transactions on Applied Superconductivity*, vol. 29, no. 5, p. 4603405, Aug 2019.

[23] J. G. Storey, A. E. Pantoja, Z. Jiang, R. A. Badcock, and C. W. Bumby, "Optimizing rotor speed and geometry for an externally mounted HTS dynamo," *IEEE Transactions on Applied Superconductivity*, vol. 29, no. 5, p. 5202705, Aug 2019.

[24] J. Ma, J. Geng, J. Gawith, H. Zhang, C. Li, B. Shen, Q. Dong, J. Yang, J. Chen, Z. Li, and T. A. Coombs, "Rotating permanent magnets based flux pump for HTS no-insulation coil," *IEEE Trans. Appl. Supercond.*, p. 8663420, 2019.

[25] S. Han, J. Lee, H. Jeon, H. M. Kim, J. H. Kim, Y. Jo, H. Kim, T. K. Ko, and Y. S. Yoon, "Charging characteristics of rotary HTS flux pump with several superconducting wires," *IEEE Transactions on Applied Superconductivity*, vol. 29, no. 5, pp. 1–5, Aug 2019.

[26] K. Hamilton, R. Mataira, J. Geng, C. Bumby, D. Carnegie, and R. Badcock, "Practical estimation of HTS dynamo losses," Sept 2019, submitted to IEEE Trans. Appl. Supercond. proceedings MT26 Tue-Af-Po2.16-02.

[27] R. C. Mataira, M. D. Ainslie, R. A. Badcock, and C. W. Bumby, "Origin of the dc output voltage from a high-tc superconducting dynamo," *Applied Physics Letters*, vol. 114, no. 16, p. 162601, 2019.

[28] A. M. Campbell, "A circuit analysis of a flux pump," *Superconductor Science and Technology*, 2019.

[29] Z. Jiang, C. W. Bumby, R. A. Badcock, H.-J. Sung, N. J. Long, and N. Amemiya, "Impact of flux gap upon dynamic resistance of a rotating HTS flux pump," *Supercond. Sci. Technol.*, vol. 28, no. 11, p. 115008, 2015.

[30] J. Geng, B. Shen, C. Li, H. Zhang, K. Matsuda, J. Li, X. Zhang, and T. A. Coombs, "Voltage-ampere characteristics of YBCO coated conductor under inhomogeneous oscillating magnetic field," *Appl. Phys. Lett.*, vol. 108, no. 26, p. 262601, 2016.

[31] S. Bilicz, "Approximate and proper electromagnetic modelling in moving conductors," *Period. Polytech. Elec. Eng. Comp. Sci.*, vol. 59, no. 2, pp. 43–47, 2015.

[32] K. Kajikawa, T. Hayashi, R. Yoshida, M. Iwakuma, and K. Funaki, "Numerical evaluation of ac losses in HTS wires with 2D FEM formulated by self magnetic field," *IEEE Trans. Appl. Supercond.*, vol. 13, no. 2, pp. 3630–3633, June 2003.

[33] Z. Hong, A. M. Campbell, and T. A. Coombs, "Numerical solution of critical state in superconductivity by finite element software," *Supercond. Sci. Technol.*, vol. 19, no. 12, pp. 1246–1252, 2006.

[34] R. Brambilla, F. Grilli, and L. Martini, "Development of an edge-element model for ac loss computation of high-temperature superconductors," *Superconductor Science and Technology*, vol. 20, no. 1, pp. 16–24, nov 2006.

[35] M. D. Ainslie, T. J. Flack, and A. M. Campbell, "Calculating transport ac losses in stacks of high temperature superconductor coated conductors with magnetic substrates using FEM," *Physica C: Superconductivity*, vol. 472, no. 1, pp. 50 – 56, 2012.

[36] M. D. Ainslie and H. Fujishiro, "Modelling of bulk superconductor magnetization," *Supercond. Sci. Technol.*, vol. 28, no. 5, p. 053002, mar 2015.

[37] M. D. Ainslie, C. W. Bumby, Z. Jiang, R. Toyomoto, and N. Amemiya, "Numerical modelling of dynamic resistance in high-temperature superconducting coated-conductor wires," *Supercond. Sci. Technol.*, vol. 31, no. 7, p. 074003, 2018.

[38] C. Plummer and J. Evetts, "Dependence of the shape of the resistive transition on composite inhomogeneity in multifilamentary wires," *IEEE Trans. Magn.*, vol. 23, no. 2, pp. 1179–1182, March 1987.

[39] J. Rhyner, "Magnetic properties and ac-losses of superconductors with power law current—voltage characteristics," *Physica C*, vol. 212, no. 3, pp. 292 – 300, 1993.

[40] N. Strickland, C. Hoffmann, and S. Wimbush, "A 1 kA-class cryogen-free critical current characterization system for superconducting coated conductors," *The Review of scientific instruments*, vol. 85, p. 113907, 11 2014.

[41] S. C. Wimbush and N. M. Strickland, "A public database of high-temperature superconductor critical current data," *IEEE Trans. Appl. Supercond.*, vol. 27, no. 4, p. 8000105, June 2017.

[42] K. Hamilton, A. E. Pantoja, J. G. Storey, Z. Jiang, R. A. Badcock, and C. W. Bumby, "Asynchronous magnet–stator topologies in a squirrel-cage superconducting dynamo," *IEEE Transactions on Applied Superconductivity*, vol. 29, no. 5, pp. 1–5, Aug 2019.

[43] J. Geng, K. Hamilton, R. Mataira, R. Badcock, and C. Bumby, "A kilo-ampere class "squirrel-cage" HTS dynamo," submitted to Supercond. Sci. Tech.

[44] R. C. Mataira, M. Ainslie, R. Badcock, and C. Bumby, "Mechanism of the high T_c superconducting dynamo, models and experiment." to be submitted.